



**AMPLIFICATION OF RECTANGULAR SPOUTED BEDS BY JET  
DEFLECTION**

Lappeenranta-Lahti University of Technology LUT

Bachelor's Programme in LUT-HEBUT, Bachelor's thesis

2025

Bozhen Wang

Examiner(s): Associate Professor Yuanhe Yue

D.Sc. (Tech.) Antti Pitkääja

## ABSTRACT

Lappeenranta-Lahti University of Technology LUT

LUT School of Energy Systems

Energy Technology

Double degree, In co-operation with partner university: Hebei University of Technology

Bozhen Wang

### **Amplification of rectangular spouted beds by jet deflection**

Bachelor's thesis

2025

46 pages, 21 figures, 5 tables and 4 appendices

Examiner(s): Associate Professor Yuanhe Yue

D.Sc. (Tech.) Antti Pitkääoja

Keywords: Deflected spouting, Spouted bed, Scale-up design

Spouted beds were first proposed in the 1950s, and have been refined and updated in various ways, and are now in their development period, but there are still problems with jet deflection. This study takes the rectangular spouted bed as the object and systematically analyzes the influence of the nozzle position on the particle movement behavior and jet deflection and distribution. Setting three cases with different nozzle position which  $D=0.12$  m,  $D=0.14$  m and  $D=0.16$  m. Then each run for 50 seconds and then find the optimal nozzle position with compared the result such as particle distribution and residence time. The simulation results show that the appropriate optimization of the nozzle position can significantly reduce the jet deflection phenomenon and improve the uniformity of particle distribution. This complete design not only ensures the Controllability of experimental conditions but also provides a reference for the construction and optimization of future small-scale test devices. The characteristics of this study are setting different nozzle positions in the system to obtain comprehensive comparative analysis results, third combing simulation with engineering design, take into account both theoretical research and actual application which reflecting a high degree of maturity and engineering feasibility.

## SYMBOLS AND ABBREVIATIONS

### Roman characters

$p$	pressure	bar, Pa
$qm$	mass flow rate	kg/s
$R$	gas constant	J/kg K
$T$	temperature	°C, K
$U$	voltage	V
$V$	volume	m <sup>3</sup>
$v$	specific volume	m <sup>3</sup> /kg
$x$	vapour content	
$U_{min}$	Minimum spouting velocity	m/s
$H_{max}$	Maximum spouted bed height	m
$\Delta p$	Pressure drop	Pa
$D$	Bed or nozzle diameter	m
$Dp$	Particle diameter	m
$x$	Vapor content	–
$C$	Empirical coefficient	–

### Greek characters

$\lambda$	thermal conductivity	W/mK
$\theta$	Incidence angle (if applicable)	–
$\mu$	Dynamic viscosity	Pa·s
$\rho$	Density (gas or particle)	kg/m <sup>3</sup>

$\eta$  Efficiency or porosity –

#### Constants

$g$  gravitational acceleration 9,81 m/s

#### Dimensionless quantities

$Re$  Reynolds number

$Ar$  Archimedes number

$\varepsilon$  Void fraction/porosity

#### Subscripts

1 inflow

2 outflow

mit measured

ms Minimum spouting

p Particle

g Gas

#### Abbreviations

CFD Computational Fluid Dynamics

DEM Discrete Element Method

DPM Discrete Phase Model (in Fluent)

TGA Thermogravimetric Analysis

SST Shear Stress Transport (Turbulence Model)

CT Computed Tomography

RPT      Radioactive Particle Tracking

## Table of contents

Abstract

(Symbols and abbreviations)

1	Introduction .....	8
1.1	Background and Motivation.....	8
1.2	Application of spouted beds in energy, chemistry and materials processing. ....	9
1.3	Phenomenon and mechanism of jet deflection in rectangular spouted bed .....	10
1.4	Disadvantages and challenges of spouted bed .....	10
1.5	Industrial application and scale-up of spouted fluidized bed.....	11
1.6	Current research status .....	13
1.7	Research Purpose and Significance .....	15
2	Brief Introduction to Fluid Dynamics Indexes of Spouted Bed .....	15
2.1	Fluid dynamics of spouted bed .....	15
3	Structural size design calculation .....	18
3.1	Basic governing equations .....	19
3.1.1	Gas phase governing equations.....	19
3.1.2	Solid phase governing equations .....	20
3.1.3	Dynamic interaction between gas and solid phases.....	20
3.2	Simulation parameter design.....	21
3.2.1	Numerical simulation and boundary conditions .....	21
3.2.2	Case settings in simulation .....	22
3.2.3	Determination of structural dimensions.....	23
3.3	modeling.....	24
3.4	Simulation .....	24
3.5	Simulation Results Analysis of three cases.....	25
3.5.1	Result analysis of case 1 .....	25
3.5.2	Result analysis of case 2 .....	27
3.5.3	Result analysis of case 3 .....	28
3.5.4	Particle velocity vector diagram analysis .....	30

3.5.5	Pressure Drop Plotting and Analysis .....	31
3.5.6	Particle residence time analysis .....	34
3.5.7	Comprehensive simulation result analysis.....	36
4	Conclusions .....	36
	References.....	38

## Appendices

Appendix 1. Granular injection file

Appendix 2 Calculate the pressure drop of case 1

Appendix 3 Calculate the pressure drop of case 2

Appendix 4 Calculate the pressure drop of case 3

# 1 Introduction

## 1.1 Background and Motivation

A spouted bed is a fluidized bed under special conditions and a special type of gas-solid contact equipment. Spouted bed technology originated in the 1950s and was invented by Gisher P.E. of Canada and Mathur K.B. of India (Mathur & Epstein, 1974). It was initially used in the drying process of large particles such as wheat. The basic structure of the original spouted bed is shown in figure 1.

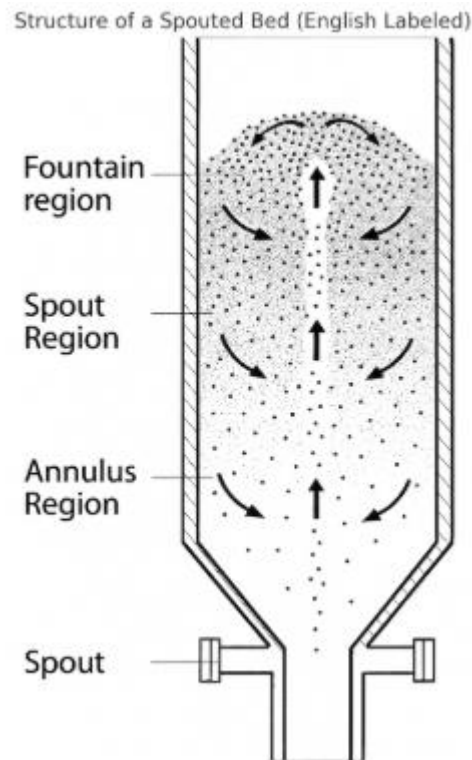


Figure 1. Traditional spouted bed structure.

Figure 1 shows a typical cross-sectional view of a spouted bed structure. The spouted bed is filled with large particles such as wheat. The nozzle at the bottom is the inlet area for gas to enter the spouted bed. The gas velocity is high, forming a local high-speed airflow to push the particles up and provide power for the entire system. The jet penetrating the bed will form three areas with different flow structures, namely the dilute phase jet area, the dense

phase annular gap area and the fountain area. The jet area is in the middle and lower part of the spouted bed. The high-speed airflow passes through this area to form an "air column", which blows the particles up through strong power to form an upward particle jet. The fountain area is located at the top of the spouted bed. The airflow and particles passing through the jet area slow down after arriving here and fall into the annular gap area on both sides according to a parabolic trajectory, thereby forming an annular reflux. (Mathur & Gisher, 1955).

## 1.2 Application of spouted beds in energy, chemistry and materials processing.

With the joint efforts of many scientists and scholars, spouted bed technology has been gradually improved and has been gradually applied to multiple industrial fields, especially in energy conversion, chemical reaction processes and material preparation. In more detail, spouted beds have been gradually applied to coal gasification, biomass pyrolysis, granulation and coating, material drying and mixing, coal combustion and flue gas desulfurization, iron ore reduction and other fields (Wu et al., 2020). The application in the energy field is mainly concentrated in biomass gasification, coal powder drying and combustion, and heat recovery and heat exchange devices. In the entire energy system, it can improve system efficiency, reduce energy consumption and better adapt to the ability of complex particle materials (Boujjat et al., 2020). The application in the chemical industry is mainly reflected in the fact that as a catalytic reactor, the spouted bed can provide good gas-solid mixing and controllable residence time for the catalytic reaction. The classic example is Fischer-Tropsch synthesis and hydrocracking. Other aspects can also be used for rapid drying and coating of powder products. In summary, the high response speed and continuous operation capability brought by the spouted bed in the chemical industry are the advantages of the spouted bed (Orozco et al., 2021). The application in material processing mainly lies in powder coating and encapsulation, nanoparticle granulation and sintering pretreatment, and metal particle heat treatment and reaction. We all know that functional materials, ceramics and metal powders occupy a large part of our daily life, and the spouted bed can just improve the properties of these fine materials.

### 1.3 Phenomenon and mechanism of jet deflection in rectangular spouted bed

At present, the spouted bed is widely used in various industrial processes due to its excellent gas-solid contact performance. The spouted bed has excellent gas-solid contact performance due to its unique particle circulation movement, which is caused by the jet and bed gravity effect. However, unstable particle circulation occurs in the deflected jet (San José et al., 2006). The deflected jet phenomenon refers to the phenomenon that the fluid deviates from the original direction of movement due to External airflow or temperature disturbances or own jet instability after being ejected from the nozzle. This phenomenon occurs for the most widely used conical and rectangular spouted beds on the market (Yue et al., 2021).

When the spouted bed is running stably, the spouted fluidized bed can be divided into three areas: the high-speed airflow in the jet zone carries the particles upward, and the particles in the fountain zone scatter to both sides after reaching the top, so these two areas are both dilute phases (Mathur & Epstein, 1974). The annular gap area is a dense phase. At this time, there are clear boundaries between the three areas, and the circulation of the particles is stable and orderly, but in the case of a multi-nozzle spouted bed, this stable state is easily broken by deflected jetting. Through theoretical analysis, hypothesis and simulation verification proposed two causes of deflected jet (Yue et al., 2021). First, the asymmetric distribution of particles during the jetting and falling process will cause the jet to deflect. Second, the rheological properties of the particles in the annular gap will also affect the jet deflection. On this basis, scientists further characterized and quantified the deflected jet and proposed an innovative jet deflection angle based on the scale of microscopic particles. This jet deflection angle can be accurately quantified by measuring the velocity vector deflection angle of the particle or gas phase during injection.

### 1.4 Disadvantages and challenges of spouted bed

Spouted beds also have inherent disadvantages: in the process of fluidization, the particles of traditional spouted beds cannot be completely and evenly fluidized, and local particle agglomeration and mesoscale structures will appear, resulting in changes in heat transfer properties and affecting the working efficiency of the reaction (Sutkar et al., 2013; Zhong et al., 2016). Spouted beds are usually only suitable for large particles and high-density

particles. For small or light particles, the use of spouted beds is prone to fly upward, insufficient mixing or bed instability; due to the limitation of geometric size, large-scale cannot be achieved; when the operating gas velocity is unstable, the ejected fluid may deviate, collapse or block; the particle circulation efficiency is low and the spouting range is small, which causes the material in the bed to stay for a long time, which has an adverse effect on the heat and mass transfer efficiency of drying; high-speed airflow and particle circulation during long-term operation will cause scouring, wear and erosion of the inner wall of the equipment. To overcome these shortcomings of traditional spouted beds, various improved spouted bed types have emerged in recent years (Saidutta and Murthy 2000).

The existing spouted beds operate very stably at a small or laboratory scale, but face more complex problems and challenges when expanding scale and industrial application: the annular gap recirculation path may be interrupted due to gas-solid flow asymmetry, resulting in weakened particle circulation or even dead zones; in a multi-nozzle spouted bed, due to the large number of nozzles, interference between jets is easy to occur, and jet asymmetry can also seriously damage the particle distribution and mixing state (San José et al. 2006).

in industrial applications, the gas velocity required to maintain the jet is much higher than that of the fluidized bed, reducing the economy; there is no agreed scale-up design standard for the size of the spouted bed, and the size needs to be re-optimized; even though the spouted bed has a unique gas-solid circulation and high heat transfer efficiency, it still has many shortcomings, so the method of studying jet deflection still requires a lot of optimization (Hosseini et al., 2009).

### 1.5 Industrial application and scale-up of spouted fluidized bed

Industrial application of spouted fluidized bed in Drying of polyethylene granules. Polyethylene granules will carry excess water or residual solvent (such as isobutane, hexane, etc.) after polymerization reaction, so they need to be dried. In this process, the spouted fluidized bed drying system performs well (Jittanit et al., 2010). The exact process is shown in Figure 2.

Before entering the spouted bed, the granules must first pass through a gas-solid separator, of which the most important gas-solid separator is a cyclone separator or a centrifuge, which

will initially remove residual gas or solvent from the granules. Then the preliminarily separated granules are passed into the spouted bed from the top of the spouted bed, and high-temperature dry air is injected from the bottom nozzle of the spouted bed to form a high-speed jet to drive the granules to circulate. In the spouted bed, the granules are driven up by the high-speed gas through the jet zone, fall after entering the fountain zone, and then flow back from the annular zone, which forms a circulation of the granules. The mechanism is that the granules are in continuous contact with the hot air during the flow process, so that the water evaporates quickly. The presence of inert gas in the spouted bed is necessary. Inert gas has the functions of preventing the explosion of combustible gas, protecting the thermal stability of materials, and improving the controllability of drying.

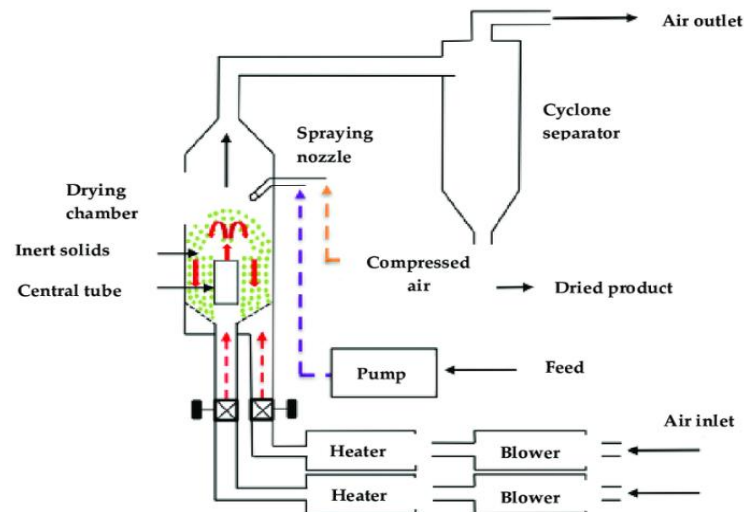


Figure 2. Spouted bed using inert gas for drying.

Nowadays, many polyolefin factories have adopted spouted beds to dry polyethylene products. In China, many factories such as Sinopec, SABIC, and BASF have put them into use. The moisture content of the dried polyethylene particles can usually be controlled at  $\leq 0.05 \text{ wt}\%$ , which can meet the requirements of molding processes such as extrusion and film blowing. The Figure 2 is a typical spouted bed containing inert gas for drying (Ostrovskij, 2014).

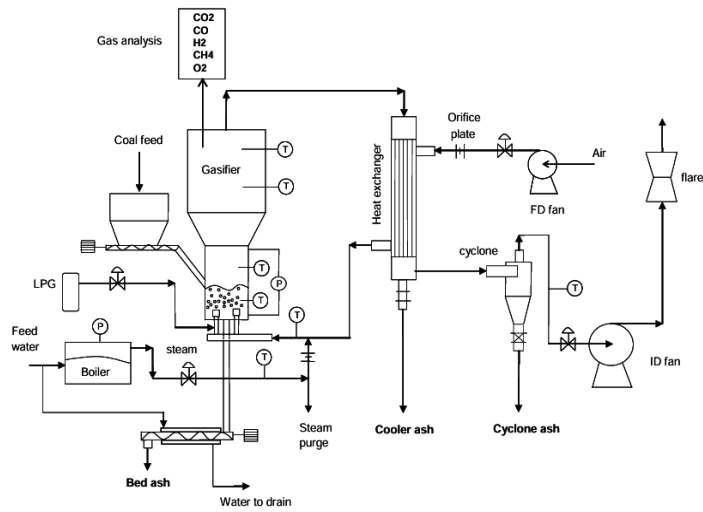


Figure 3. Flow chart of pilot fluidized bed gasifier.

Coal gasification is a technology for efficiently and cleanly processing coal resources and is mainly used to produce products that replace petroleum fuels or petrochemical products. Coal gasification refers to a clean energy conversion technology that converts coal into combustible gas through high-temperature reactions in an oxygen-deficient or oxygen-free environment. Spouted bed is a new technology with unique advantages developed in recent years (Foong, Lim and Watkinson, 1980). Ad Engelbrecht and his team designed a spouted bed gasification method to incorporate IGCC (Integrated Gasification Combined Cycle). In the experiment, the results of coal property analysis, thermogravimetric analysis (TGA) and pilot plant gasification tests were introduced to determine the performance of the selected coal under fluidized bed gasification conditions. Figure 3 shows the flow chart of the pilot fluidized bed gasifier in this experiment.

### 1.6 Current research status

The spouted bed technology was first proposed by Mathur and Gishler (1955). Since then, it has been widely studied and put into industrial application in Japan, Europe and the United States. At present, the spouted fluidized bed has become a popular device widely used in industry due to its excellent performance, and many scholars at home and abroad have done a lot of in-depth work on it (Du, Wu and Ma, 2023).

Gamliel, David P's team designed a new conical spout bed reactor for rapid catalytic pyrolysis (Gamliel et al., 2015). Antunes, Gabriella Goncalves Borges' team combined experiments and CFD-DEM simulations to systematically analyze the complex turbulent multiphase flow behavior and dynamic characteristics of particles in a pseudo-two-dimensional spouted bed under different operating conditions (Antunes et al., 2024).

Thaar Al-Juwaya adopted a newly developed mechanical scale-up method for gas-solid sprayed beds based on matching of radial distribution of gas content, and used two-scale sprayed beds of different sizes to study three groups of conditions, including large-scale reference operating conditions, radial distribution of gas content similar to the reference operating conditions, and radial distribution of gas content of small-scale sprayed beds (Al-Juwaya, Ali and Al-Dahhan, 2023). The results confirmed the effectiveness of the scale-up method in terms of dimensionless values of nozzle diameter, cumulative probability distribution of solid particles entering the nozzle, cycle time fraction of each area of the bed, radial distribution of dimensional values of root mean square particle velocity, and solid eddy diffusion rate. M. Karimi used a multilayer perceptron (MLP) neural network to accurately predict the hydrodynamic characteristics of the sprayed bed, completed a relatively large number of experiments, and used Buckingham's theorem to extract the most influential dimensionless group, establish an MLP model, and simultaneously estimate the working and peak pressure drops, providing more accurate operation and peak pressure drop information for the design, optimization, control and scale-up of the sprayed bed (Karimi et al., 2021). Neven Ali used gamma-ray computed tomography (CT) technology based on two sizes of spouted beds to evaluate a new mechanism scale-up method for gas-solid spouted beds by locally measuring the time-averaged cross-sectional distribution of solid and gas contents and their radial distribution along the bed height (Ali, Aljuwaya and Al-Dahhan, 2019). Shreekanta Aradhya proposed and verified a mechanism scale-up method for gas-solid spouted beds based on maintaining the similarity of the radial distribution of gas content (Aradhya, Taofeeq and Al-Dahhan, 2016). Neven Ali used radioactive particle tracking (RPT) to conduct an advanced evaluation of the scale-up of TRISO nuclear fuel particle coating spouted beds (Ali, Al-Juwaya and Al-Dahhan, 2017).

## 1.7 Research Purpose and Significance

Although the spouted fluidized bed has been widely used in the industrial field, it is still far from real industrial practice. The working characteristics of the spouted bed are to introduce high-speed jet gas in the center of the bed and form a symmetrical particle circulation inside the bed. At the same time, through the auxiliary effect of the light fluidizing gas, the fluidization of the particle-dense area is effectively driven. However, due to the difference in the velocity of the inlet gas, multiple fluidization states may appear in the bed, resulting in reduced system stability (Olazar et al. 1993). Therefore, the operating range of stable fluidization is very limited. In addition, due to the various geometric structures of the spouted fluidized bed, the current popular ones are mainly divided into conical spouted fluidized beds and two-dimensional spouted fluidized beds. However, only conical fluidized beds are used in industrial applications. Scientists found that the stable fluidization of the conical spouted fluidized bed is closely related to the particle diameter and the bottom jet inlet diameter. Therefore, the biggest problem facing the conical spouted fluidized bed is how to achieve amplification (Sutkar et al. 2013).

This paper aims to study the effects of different nozzle positions on gas-solid mixing performance and deflection, and to find the optimal nozzle position. Since existing spouted bed research mainly focuses on symmetrical circular beds, the research on asymmetric jet behavior in multi-nozzle rectangular spouted beds is relatively weak. This study can fill the theoretical gap in the jet deflection mechanism. This paper also optimizes the structural dimensions of the spouted bed.

## 2 Brief Introduction to Fluid Dynamics Indexes of Spouted Bed

### 2.1 Fluid dynamics of spouted bed

In the process of studying spouted beds, due to the special structure and spouting mechanism of spouted beds, fluid dynamics indicators have become an important support for analyzing the operating status, performance evaluation and structural optimization of spouted beds. In general studies, the following parameters are generally used to describe the fluid dynamics

characteristics: minimum spouting velocity, maximum spouted bed height, pressure drop, particle circulation velocity and bed expansion height (Olazar et al. 1993). Despite the fact that scientists have carried out a lot of research on the hydrodynamic properties of the ejector bed and have given many formulas related to the derivation of the research, the hydrodynamic properties of the ejector bed are still affected by many other factors such as the actual operating parameters, the choice of experimental materials, and the specific configuration of the equipment.

In a spouted bed, the minimum spouting velocity refers to the minimum gas velocity required to bring particles from the nozzle into a stable spouting state. It is an important parameter that reflects the operating status of a spouted bed. When the gas velocity is less than the minimum spouting velocity, the gas flow cannot break through the bed resistance and therefore cannot form a stable gas-solid rising jet. The following is a common empirical formula (Mathur & Gisher 1955):

$$U_{ms} = C * \left( \frac{d_p^2 * (\rho_p - \rho_g) * g}{\rho_g} \right)^{0.5} \quad (1)$$

$U_{ms}$ : minimum jet velocity (m/s),  $d_p$ : particle diameter,  $\rho_p, \rho_g$ : particle and gas density

$g$ : gravity acceleration,  $C$ : empirical coefficient, depends on bed type, nozzle diameter, etc. (usually between 0.5-1.0) (Kunii and Levenspiel, 1991).

When the structure of the spouted bed is determined, when the height of the particles in the bed exceeds a maximum limit, no matter how the gas velocity is adjusted, the spouting state in the spouted bed cannot be spouted but directly converted into bubbling or surging. The maximum limit of the bed particle accumulation currently is the maximum spouted bed height  $H_{max}$ . The following is an empirical formula for calculating the maximum spouted bed height:

$$H_{max} = \frac{D^2}{d_p} \left( \frac{D}{D_i} \right)^{\frac{2}{3}} \frac{568b^2}{Ar} \left( \sqrt{1 + 35.9 * 10^{-6} Ar} - 1 \right)^2 \quad (2)$$

Where  $D$  is the bed diameter or characteristic length,  $d_p$  is the particle diameter,  $D_i$  is the nozzle diameter,  $b$  is a dimensionless constant, usually related to the nozzle type or

equipment structure, and  $Ar$  is the Archimedean number which can be calculated using the following formula:

$$Ar = \frac{\rho g d_p^3 (\rho_s - \rho_g)}{\mu^2} \quad (3)$$

The pressure drop in a spouted bed is one of the most important gas-solid coupling characteristics. The pressure drop not only affects the energy consumption of the system but is also an important indicator for judging the spouting state and stability. It is usually expressed in units of Pascal ( $Pa$ ) or millimeters of water column ( $mmH_2O$ ). In a spouted bed, the particle size and density, gas velocity and jet intensity, bed height, nozzle diameter, and the structural shape of the spouted bed will all affect the pressure drop. The pressure drop of a spouted bed is usually expressed using the following estimated expression:

$$\Delta P = H * (1 - \varepsilon) * \rho_p * g \quad (4)$$

Where is the pressure drop,  $H$  is the bed height,  $\varepsilon$  is the porosity,  $\rho_p$  is the particle density, and  $g$  is the gravitational acceleration.

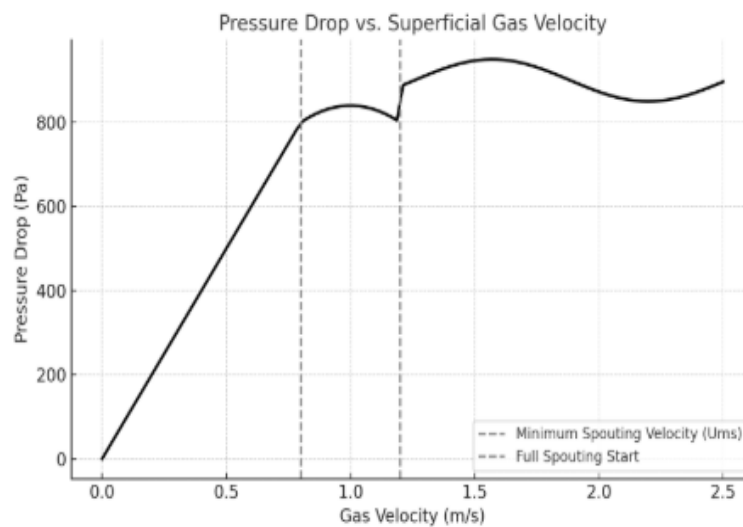


Figure 4. Pressure drop-gas velocity characteristic curve (Sutkar et al., 2013).

Figure 4 is a pressure drop-gas velocity characteristic curve, in which the spouted bed operation is divided into three stages: the pressure drop in the fixed bed stage increases

linearly with the gas velocity, the pressure drop peak appears at the critical spouting point, and a jet is formed. In the fully spouting state (greater than 1.2m/s), the pressure drop tends to be stable and slightly fluctuates (Sutkar et al., 2013).

During the operation of the spouted bed, the particles will rise through the jet zone, reverse at the top of the fountain zone, and fall through the annular zone. The speed of the particles in these processes is different. The particle circulation speed refers to the average movement speed reflected in the completion of this entire cycle.

After the spouting of the spouted bed begins, the airflow entering the center of the bed from the nozzle forms a jet, which drives the particles in the bed upward. In this process, the volume of the entire bed particles expands rapidly, and the bed height increases significantly with the increase in gas velocity. This is the actual bed height formed by the expansion of the particles driven by the bed, which is the bed expansion height.

### 3 Structural size design calculation

With the continuous advancement of computer technology, especially the rapid development of computational fluid dynamics (CFD), researchers have gradually turned from traditional experimental methods to efficient numerical simulation methods to solve problems in the study of fluid mechanics and heat transfer characteristics of spouted beds, especially in the design and research of gas-solid two-phase or multi-phase spouting states. Usually, based on establishing physical and mathematical models that conform to actual working conditions, CFD simulation software can be used to comprehensively analyze and predict the flow field characteristics, particle behavior and related influencing factors of spouted beds under different operating conditions, thereby providing a reliable basis for structural optimization and parameter adjustment.

Based on the traditional CFD method, this paper studies the flow characteristics and gas-solid mixing performance of rectangular spouted beds, focusing on the influence of different nozzle positions on jet deflection and particle movement. Due to limited space, this paper only gives a brief description.

### 3.1 Basic governing equations

In nature, fluid flow follows all natural laws, especially the laws of conservation of mass, momentum and energy. To accurately describe the flow characteristics of gas-solid two-phase in a spouted bed, the gas phase motion is solved using the continuity equation and the Navier-Stokes equation model, and the motion of solid particles is solved using Newton's second law and the rotation equation. The following is a brief introduction to the relevant equations.

#### 3.1.1 Gas phase governing equations

In the numerical simulation of the spouted bed, the gas phase as a continuous medium must satisfy the two laws of conservation of mass and conservation of momentum.

Continuity equation (mass conservation equation):

$$\frac{\partial(\varepsilon_f \rho_f)}{\partial t} + \nabla * (\varepsilon_f \rho_f \mu_f) = 0 \quad (5)$$

where the gas volume fraction is the density of the fluid, and the velocity of the calculated fluid.

$$\frac{\partial(\varepsilon_g \rho_g \vec{u}_g)}{\partial t} + \nabla * (\varepsilon_g \rho_g \vec{u}_g \vec{u}_g) = -\varepsilon_g \nabla P + \nabla * (\varepsilon_g \tau_g) + \varepsilon_g \rho_g \vec{g} + \vec{F}_{gs} \quad (6)$$

This is the momentum conservation equation and the Navier-Stokes equation, where  $P$  is the gas phase static pressure,  $u_g$  is the gravity acceleration vector, and  $F_{gs}$  the coupling force between the gas and the particle.

When the fluid phase moves, its kinetic energy will be lost due to the inherent viscosity of the fluid. At the same time, shear deformation between the fluid layers will be caused during the fluid movement. Its stress tensor  $\tau_f$  is closely related to the velocity gradient and fluid viscosity, and its expression is:

$$\tau_f = - \left[ \mu_f (\nabla u_f + (\nabla u_f)^T) + \left( \lambda_f - \frac{2}{3} \mu_f \right) (\nabla * u_f) I \right] \quad (7)$$

### 3.1.2 Solid phase governing equations

In the spouted bed discrete element method (DEM), the motion trajectory of solid particles is involved. The discrete element method simulates the interaction between particles and between particles and the wall by tracking the trajectory of each particle. Therefore, we need the translation control equation:

$$m_i \frac{d\vec{v}_i}{dt} = \vec{F}_{c,i} + \vec{F}_{g,i} + \vec{F}_{d,i} \quad (8)$$

This equation represents the translational motion equation of a particle in three-dimensional space, indicating that the velocity of a particle changes over time due to the combined force. The three force terms on the right side of the equation are contact force, gravity, and the drag exerted by the fluid on the particle.

The rotation control equation is:

$$I_i \frac{d\vec{\omega}_i}{dt} = \vec{T}_i \quad (9)$$

This equation represents the conservation of angular momentum of the particle rotating around itself. If the rotation and friction between particles are considered, the rotation control equation must be considered, especially when there is a high concentration and multiple particle collisions in the spouted bed.

### 3.1.3 Dynamic interaction between gas and solid phases

In the spouted bed gas-solid multiphase system, the momentum transfer process between the solid phase and the gas phase includes resistance and pressure difference force. At the same time, since the diameter of the studied particles is relatively large and the density of the particles is much higher than that of the fluid phase, this study did not take the gas turbulence force into account. The most important dynamic force of gas on particles is the drag force. In the DEM model, the gas drag force on particles is expressed by the following formula (Zhou et al., 2017):

$$\vec{F}_{d,i} = \frac{1}{8} C_D \pi D_p^2 \rho_g \varepsilon_g^{-2.65} |\vec{u}_g - \vec{V}_i| (\vec{u}_g - \vec{V}_i) \quad (10)$$

This study further modifies the  $CD$  model:

$$C_D = \frac{24}{Re_p} (1 + 0.15Re_p^{0.687}), Re_p < 1000 \quad (11)$$

Where  $C_D$  is the drag coefficient of a single particle;  $Re$  is the Reynolds number of the particle.

## 3.2 Simulation parameter design

### 3.2.1 Numerical simulation and boundary conditions

Table 1. physical parameters and numerical parameters

parameter	Numeric	unit
geometry	-	-
width	200x300	mm
hight	1700	mm
Total number of grid cells	96159	(-)
Solid Phase	-	-
Particle size	2	mm
Particle density	1500	kg/m <sup>3</sup>
Number of particles	36000	
Gas Phase	-	-
Gas density	1.225	kg/m <sup>3</sup>
Gas dynamic viscosity	1.7894×10 <sup>-5</sup>	Pa•s
Gas volume viscosity	0	Pa•s
pressure	101325	Pa
Particle static bed height	6.25(24500)	mm

The spouted bed used in this study is a single-nozzle spouted bed. During the spouting process of the spouted bed, the ejected air enters the internal reactor of the spouted bed from the bottom rectangular nozzle at a high speed and passes through the particles to form a path bed. The influence of background gas is not considered in this study. Table 1 shows the physical parameters and numerical parameters used in the simulation.

### 3.2.2 Case settings in simulation

Table 2. Example setting details

Case number	1	2	3
Spacing(D)	0.095	0.085	0.075
Particle density	1500	1500	1500
Gas velocity	30	30	30
Gas density	1.225	1.225	1.225
Particle size	2	2	2
Particle density	1500	1500	1500
pressure	101325	101325	101325

The numerical simulation in this paper aims to explore the effect of nozzle position on particle motion in a rectangular spray bed. Table 2 gives the relevant details of the case settings. Specifically, the spray velocity ( $U_{sp}$ ) is set to 30 m/s and the background gas velocity ( $U_{bg}$ ) is set to 0 m/s. In cases 1 to 3, the gas spray area is uniformly cut into distances of 0.06 m, 0.07 m, and 0.08 m. Here D represents the distance from the upper end of the nozzle to the edge of the spouted bed. In all the above cases, the gas temperature is set to 25 °C and the particle temperature is set to 90 °C, so that the heat of the particles is taken away by the flowing gas during the spraying process (Hooshdaran et al., 2017). The simulation results will compare the fluid dynamics characteristics of different nozzle positions in terms of void distribution rate and particle motion and evaluate the gas-solid mixing performance of the system based on particle velocity distribution, particle temperature drop rate and particle temperature change (Subramanian et al. 2003).

### 3.2.3 Determination of structural dimensions

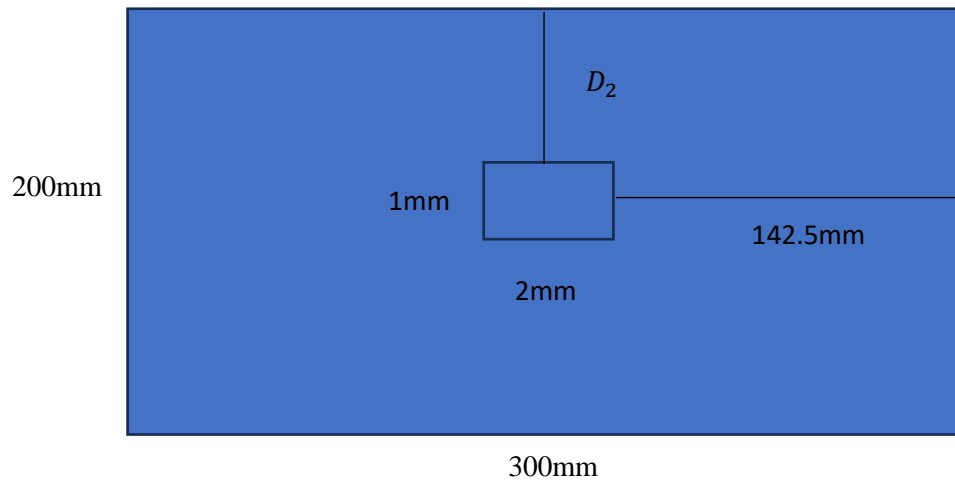


Figure 5. Design of the bottom structure of the spouted bed.

Then, according to the different  $D_2$  in the three cases set, the fluid domains are modeled and established respectively, as shown in Figure 5.

### 3.3 modeling

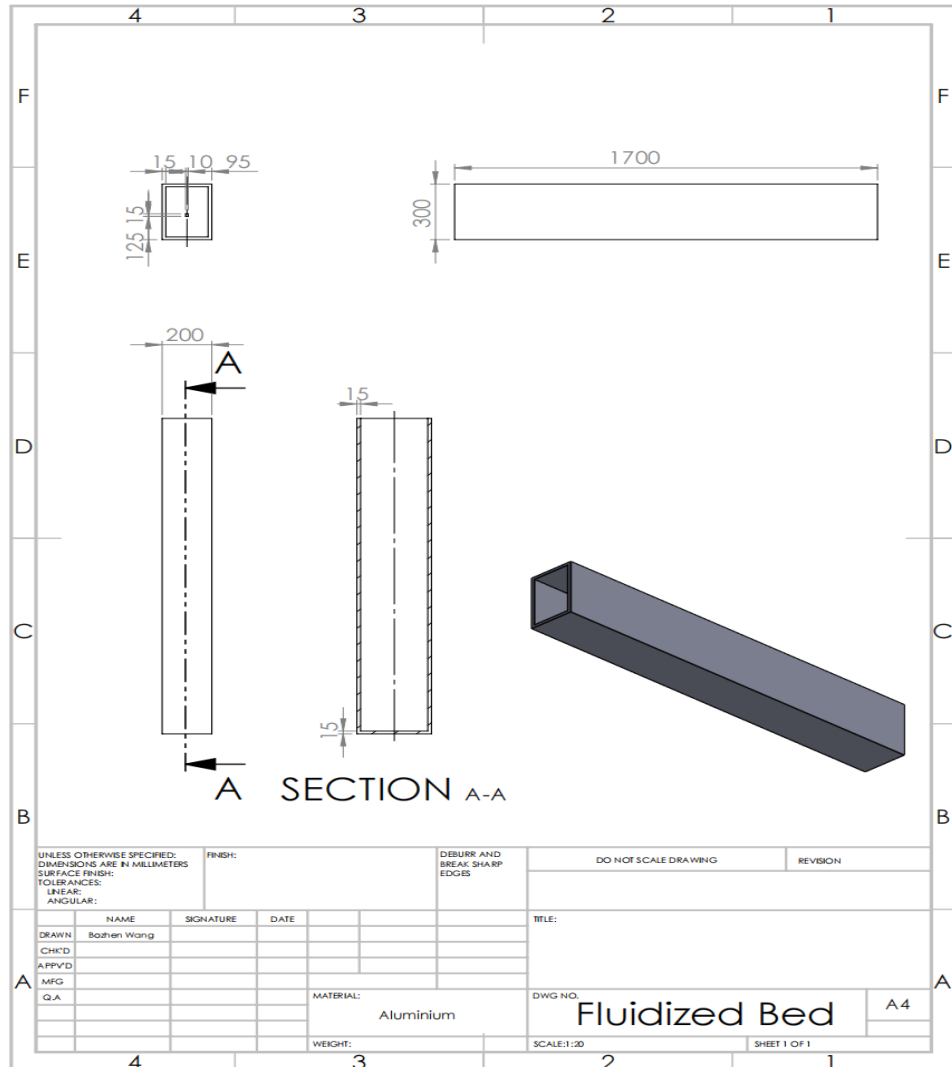


Figure 6. modeling figure.

Modeled to size, as shown in Figure 6.

### 3.4 Simulation

Before the simulation started, I set up the model in the following steps: First, select the Eulerian model for multiple models and turn on the discrete phase model. The viscosity model uses the k-omega (2 equation) model to represent that the simulation only simulates turbulence. Under the k-omega model, I further select the SST (Shear Stress Transport)

model, simulate the time as steady-state flow, then add gravity acceleration in the Y direction, and finally select Mixture for the turbulent multiphase model.

Then set up the discrete phase model, enable the interaction between the discrete phase and the continuous phase, and turn on particle injection using unsteady particle tracking, allowing particle trajectories to change over time. For this simulation, I chose to use matlab code to generate particle files (see appendix 1), generating 36,000 rows of spatial coordinates, representing 36,000 particles.

The resistance model is Wen-Yu model, and the discrete phase model is the DEM collision. In Fluent's Models panel, select Discrete Phase Model (DPM) and check the Discrete Element Method (DEM) option. The boundary conditions are inlet velocity and gauge pressure are 0 to represent all atmospheric pressures. To prevent particles from escaping from the system, a discrete-phase BC type reflect reflection is set to ensure that particles do not escape after impacting the surface.

The final solution method calculates the time step number of 500 steps, the step length is 0.1 seconds, a total of 50 seconds, and the maximum number of iterations is 20 times.

### 3.5 Simulation Results Analysis of three cases

#### 3.5.1 Result analysis of case 1

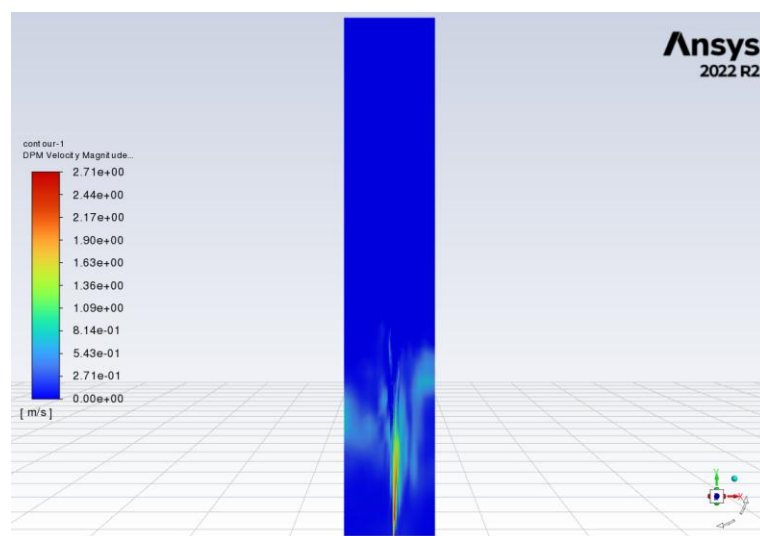


Figure 7. Fluid velocity distribution profile of case 1.

The color gradient in Figure 7 reflects the range of particle velocities from 0 m/s (stationary) to 2.71 m/s (maximum). The high velocity region (2.71 m/s) corresponds to the core area of gas injection in the center of the bed, and the low velocity region (0.27 m/s) usually appears near the wall or in the particle settling area, which shows the typical “high velocity in the center - low velocity in the periphery” characteristics of the bed flow.

Through the analysis of the fluid velocity profile of case 1, since the nozzle is almost located in the center of the bed, the velocity field obviously presents an axisymmetric structure, the injection effect is ideal, the influence of jet deflection is small, the mixing effect is good, and the structure is stable.

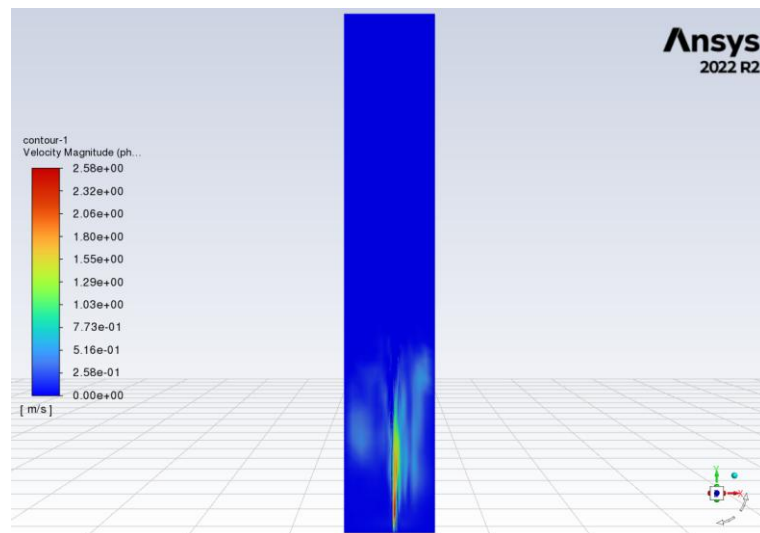


Figure 8. Particle velocity distribution profile of case 1.

The color gradient in Figure 8 shows the velocity variation in the range of 0-2.58 m/s. The high velocity region (2.58 m/s) in the figure corresponds to the center jet stream of the ejector bed, while the low velocity region (0.26 m/s) is distributed in the near-wall or particle-dense region, and this resultant figure provides an important basis for analyzing the gas-solid phase interaction.

By analyzing the particle velocity profile of case 1, it was found that the maximum velocity of the particles was 2.58 m/s, and they were mainly concentrated just above the nozzle, i.e., at the center line, and were distributed relatively evenly.

### 3.5.2 Result analysis of case 2

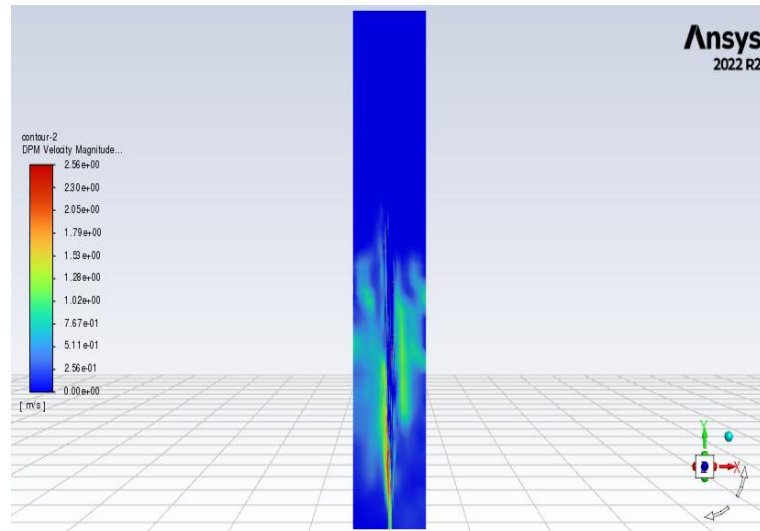


Figure 9. Fluid velocity distribution profile of case 2.

The color gradient in Figure 9 presents the characteristics of the change in the range of 0-2.58 m/s. In the figure, the maximum velocity of 2.58 m/s appears in the core injection region, while the velocity in the near-wall region decreases to below 0.26 m/s, reflecting the boundary layer effect, and meanwhile, the distribution range of the medium-velocity region of 1.03-1.80 m/s can provide an important basis for the optimization of the mixing efficiency of the reactor.

In case 2, it can be observed that due to the slight offset of the nozzle, the velocity field begins to jitter, and the high-speed area is not on the center line but offset to the left, indicating that the airflow distribution is uneven.

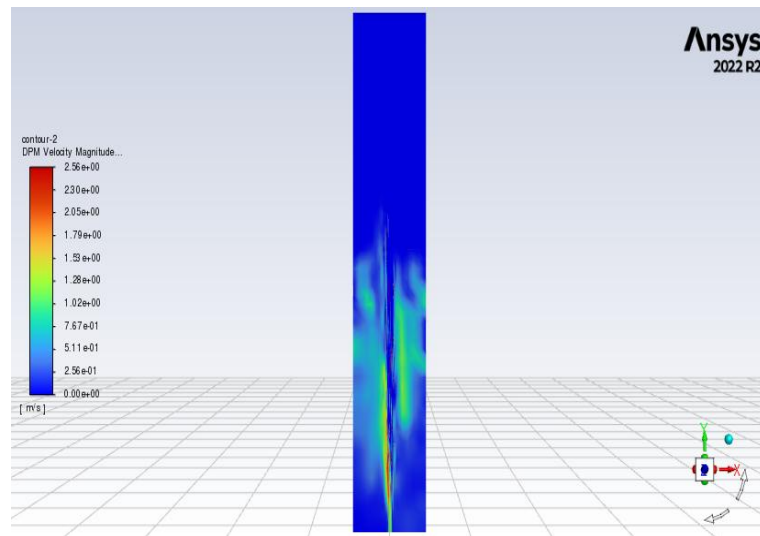


Figure 10. Particle velocity distribution profile of case 2.

The color gradient in Figure 10 shows that the effective velocity values are mainly distributed in the range of 0.06-2.5 m/s, showing a reasonable decreasing trend, but the velocity can change abruptly due to the offset of the nozzle position in case2.

In case 2, due to nozzle offset, the maximum speed is 2.56 m/s, and the high-speed area is biased to one side, indicating that jet deflection has occurred.

### 3.5.3 Result analysis of case 3

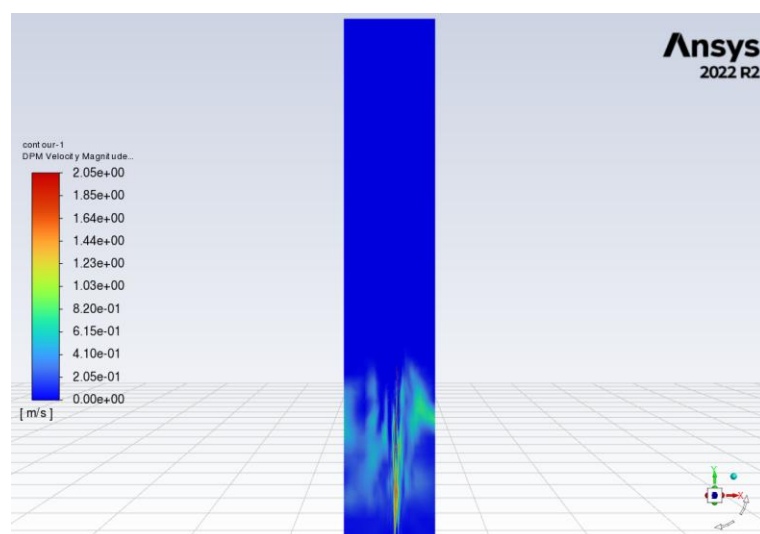


Figure 11. Fluid velocity distribution profile of case 3.

The color gradient in Figure 11 reflects the range of particle velocities from 0 m/s (stationary) to 2.05 m/s (maximum).

In case 3, since the nozzle is seriously deviated from the center point, the velocity has a serious deviation, and the velocity field jitters very seriously. One side is a high-speed area with concentrated velocity, while the other side is a completely low-speed area, and the particles are almost not fluidized (Yue et al., 2019).

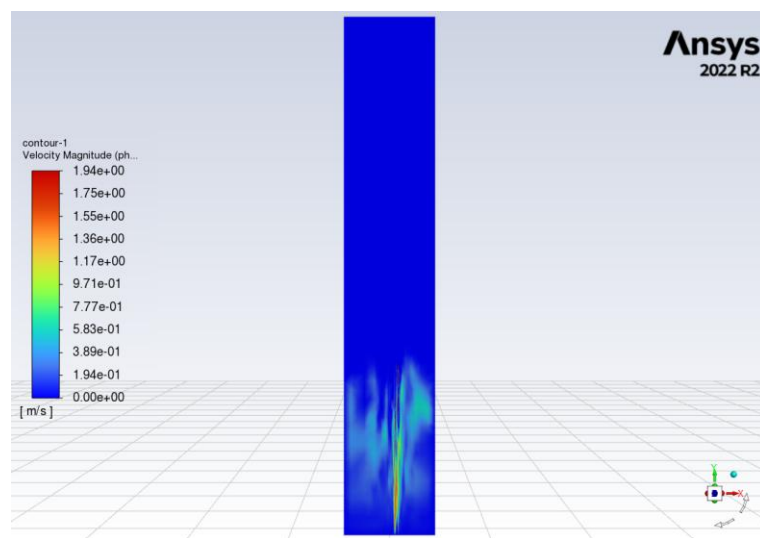


Figure 12. Particle velocity distribution profile of case 3.

The color gradient in Figure 12 reflects the range of fluid velocities from 0 m/s (stationary) to 1.94 m/s (maximum).

In the last case 3, due to the obvious nozzle offset, we found that the maximum speed was only 1.94 m/s, but the high-speed area was very concentrated, indicating that particles in other areas were restricted and stagnant or moving slowly.

### 3.5.4 Particle velocity vector diagram analysis

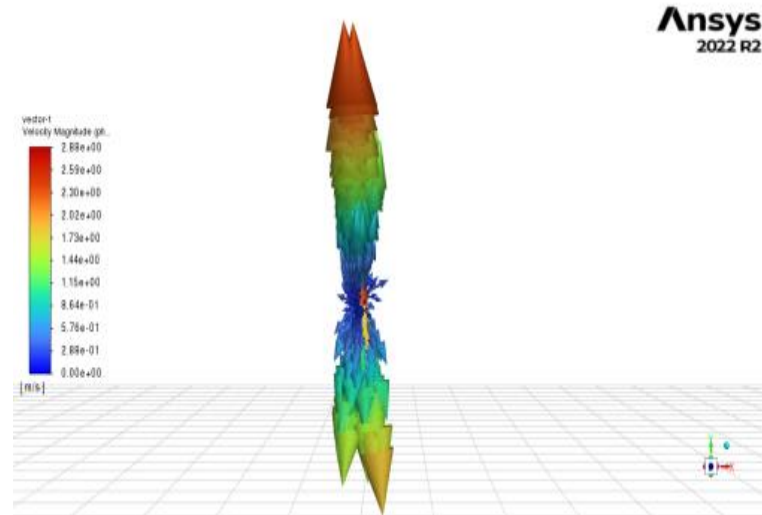


Figure 13. Case 2 Particle velocity vector diagram.

The maximum velocity of 2.8 m/s in Figure 13 occurs in the center jet region with the vector direction vertically upward, and because of the settling motion of particles in the annular zone, the velocity in the near-wall region decreases to less than 0.9 m/s, and the vector direction turns downward.

Since the velocity vector diagram of case 1 is very symmetrical, we take the velocity vector diagrams of case 2 and case 3 for analysis. From the figure, we can clearly see that the arrows at the upper and lower ends are more concentrated, indicating that the nozzle offset at this time has little effect on the symmetrical reflux structure, but there is a clear disturbance area in the middle.

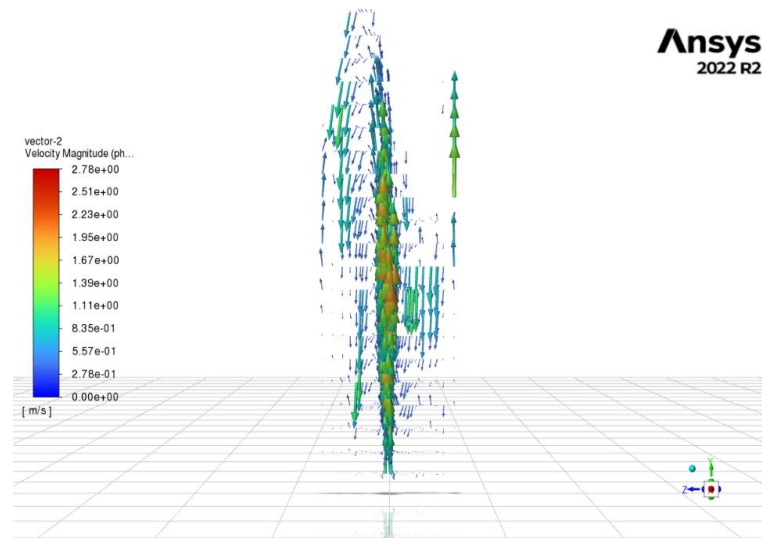


Figure 14. Case 3 Particle velocity vector diagram.

The maximum velocity of 2.78 m/s in Figure 14 occurs in the center jet region with the vector direction vertically upward, and the velocity in the near-wall region decreases to close to 0 m/s because of the settling motion of the particles in the annular region and the deviation of the nozzle position.

### 3.5.5 Pressure Drop Plotting and Analysis

Analyzing the velocity vector diagram of case 3, it can be clearly seen that the arrows are all gathered to the left, which is due to the nozzle position and the serious leftward deviation from the center point at this time, and the obvious vortex structure and lateral flow components appear, which shows that the flow pattern at this time is complex and turbulent. It is seriously affected by jet deflection.

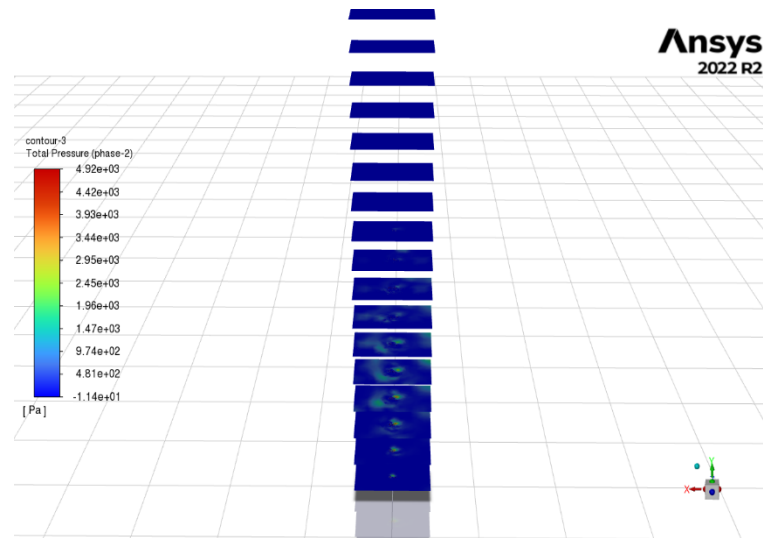


Figure 15. Plane creation.

Since the bed height of the spouted bed is 1.7 meters, I have made 16 planes from 0.1 meters to 0.17 meters at intervals of 0.1 meters as shown in Figure 15. Then the average pressure of each surface was measured and plotted into a line graph. As shown in Figure 14.

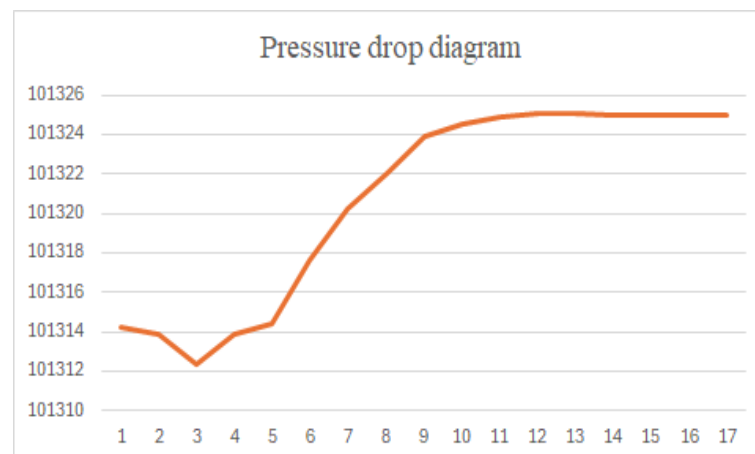


Figure 16. Pressure drop diagram in case 1.

Figure 16 is a pressure drop diagram for case 1, in which the pressure drops from 101314 Pa by about 2 Pa to 101312 Pa, and finally rises and remains at 101325 Pa.

The pressure drops distribution diagram of Case 1 shows that the gas remains stable after flowing in and the bed resistance distribution is uniform and reasonable.

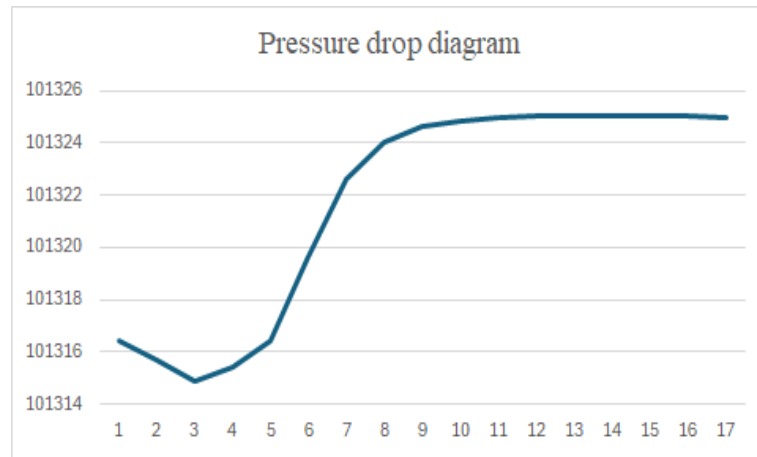


Figure 17. Pressure drop diagram in case 2.

Figure 17 is a pressure drop diagram for case 2, in which the pressure drops from 101317 Pa by about 2 Pa to 101315 Pa, and finally rises and remains at 101325 Pa.

The pressure drops distribution diagram of Case 2 shows that the initial pressure is lower, but the pressure rise trend is steeper than that of Case 1, indicating that the injection path is shorter and there is a certain amount of jet deflection.

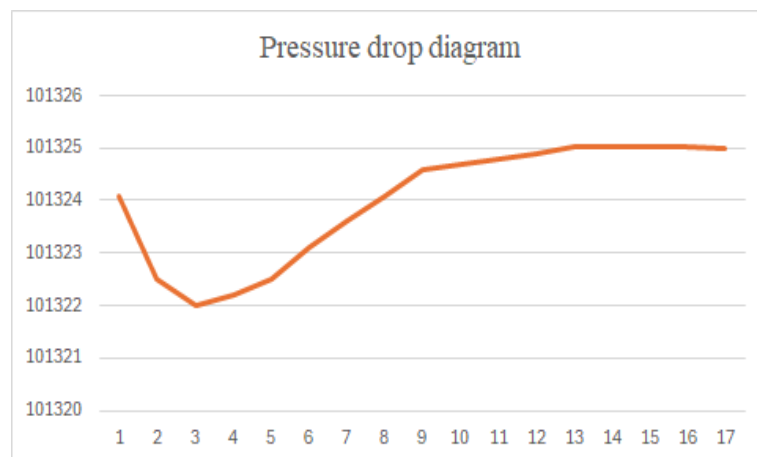


Figure 18. Pressure drop diagram in case 3.

Figure 18 is a pressure drop diagram for case3, in which the pressure drops about 2 Pa from 101324 Pa to 101322 Pa, and finally rises and remains at 101325 Pa.

### 3.5.6 Particle residence time analysis

Although the pressure drop distribution diagram of Case 3 has the most stable overall change, this shows that the airflow does not effectively penetrate the entire bed and there is particle accumulation.

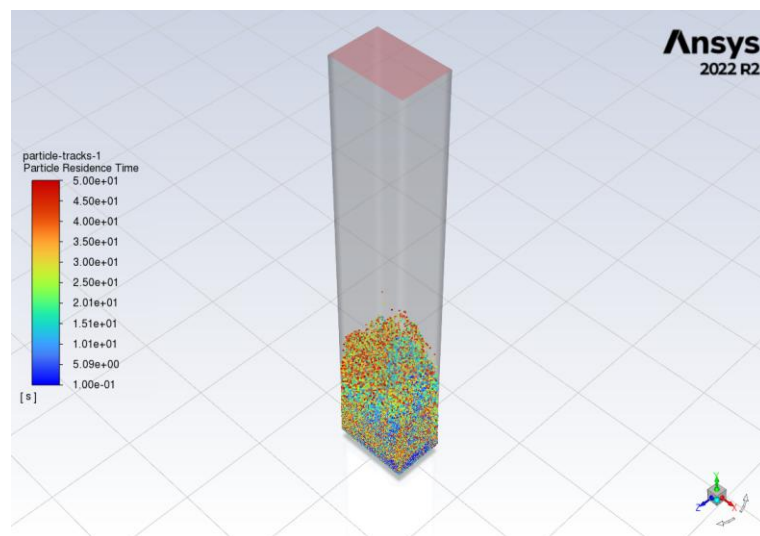


Figure 19. Particle residence time of case 1.

The time range in Figure 19 is from 1 to 50 seconds, where most of the particle residence time is concentrated in the 5-50 second interval.

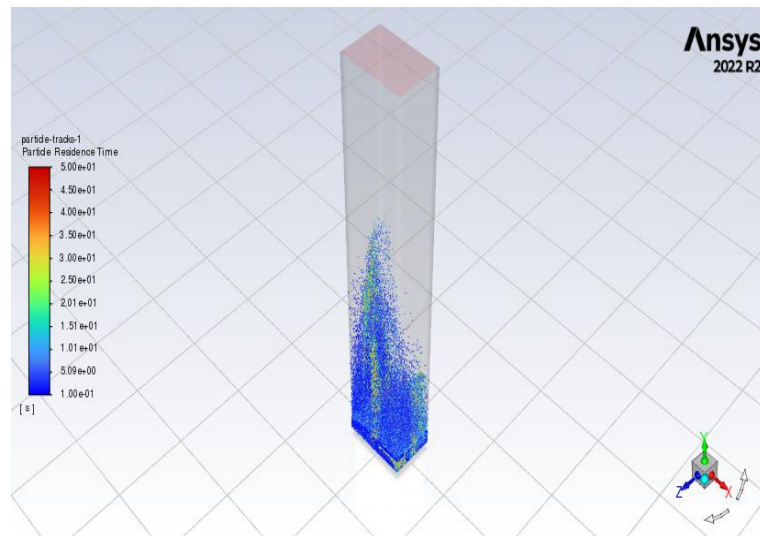


Figure 20. Particle residence time of case 2.

The time range in Figure 20 is from 1 to 50 seconds, with about 50% of the particles having residence times in the 0.25-0.5 second range, while the shortest residence time of 0.1 seconds is for particles that escape directly.

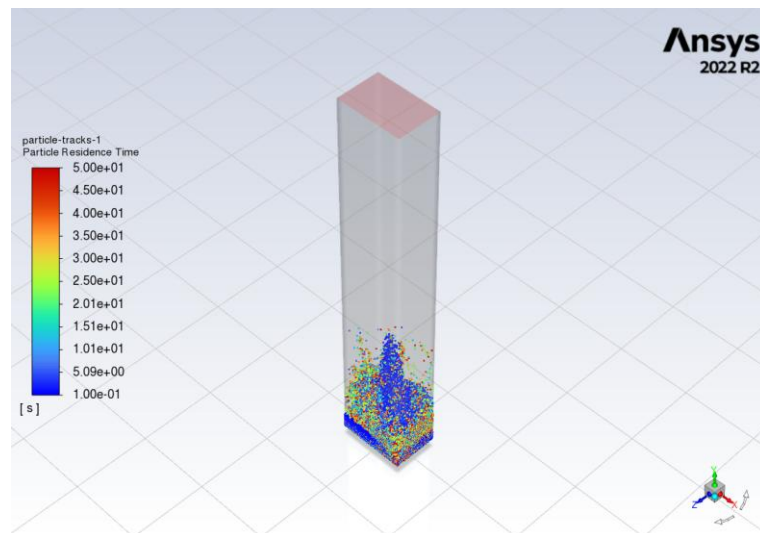


Figure 21. Particle residence time of case 3.

The time range of Figure 21 is from 1 second to 50 seconds, with about 50% of the particle residence time in the 10-50 second interval.

### 3.5.7 Comprehensive simulation result analysis

By comparing the particle residence time in the three cases, we can clearly see the effect of the nozzle position on the jet deflection. In case 1, because the nozzle position is more central, the system disturbance is small, and the particle distribution and residence time are relatively uniform. However, in cases 2 and 3, the system disturbance is enhanced, and the particles are quickly drawn into the mainstream area, and the shortened residence time indicates the effect of jet deflection. We can analyze through the particle velocity that in the case of case 1, the direction of the movement velocity is mainly vertically upward, almost maintaining the axisymmetry. In cases 2 and 3, the particle velocity increases significantly, and the offset is large, indicating that the particles are affected by the asymmetric gradient pressure and deflected.

## 4 Conclusions

This study focuses on the jet deflection phenomenon in a rectangular nozzle bed. The effect of jet position change on gas-solid flow behavior under different operating conditions is systematically analyzed by CFD simulation. The study focuses on how the change of nozzle position leads to the asymmetric deflection of the jet, which affects the key parameters such as velocity distribution, residence time, turbulence intensity and spatial distribution of particles in the bed.

By setting up three sets of typical conditions to compare the simulation results, it can be seen that: with the increase of the inlet flow disturbance, the degree of jet deflection is gradually intensified, and the particle trajectory develops from axisymmetric to significantly deviate from the direction of the central axis. In Case 1, the flow field has good symmetry, the particle residence time is long, and the jet structure is stable; in Case 2, the initial signs of deflection begin to appear, and the particle distribution is shifted; in Case 3, the jet is obviously deflected to one side, and a typical deflected jet trajectory is formed accompanied by a significant increase in the turbulent kinetic energy, an increase in the particle velocity, and a shortening of the residence time.

The results show that the jet deflection can effectively change the particle transport path and enhance the mixing and turbulence intensity in the bed, which is of positive significance for improving the gas-solid reaction, heat and mass transfer efficiency of the jet bed. This study provides numerical basis and experimental support for the jet-guided design and optimization of the jetted bed structure. The follow-up work can further combine the nozzle structure adjustment with real-time feedback control to realize the active regulation of jet deflection behavior

## References

- Al-Juwaya, T., Ali, N. and Al-Dahhan, M. (2023) ‘Experimental validation of the mechanistic scale-up methodology of gas–solid spouted beds using radioactive particle tracking (RPT)’, *Annals of Nuclear Energy*, 181, 109633.
- Karimi, M., Vaferi, B., Hosseini, S.H., Olazar, M. and Rashidi, S. (2021) ‘Smart computing approach for design and scale-up of conical spouted beds with open-sided draft tubes’, *Particuology*, 55, pp. 179–190.
- Ali, N., Aljuwaya, T. and Al-Dahhan, M. (2019) ‘Evaluating the new mechanistic scale-up methodology of gas-solid spouted beds using gamma ray computed tomography (CT)’, *Experimental Thermal and Fluid Science*, 104, pp. 186–198.
- Aradhya, S., Taofeeq, H. and Al-Dahhan, M. (2016) ‘A new mechanistic scale-up methodology for gas-solid spouted beds’, *Chemical Engineering and Processing: Process Intensification*, 110, pp. 146–159.
- Ali, N., Al-Juwaya, T. and Al-Dahhan, M. (2017) ‘An advanced evaluation of spouted beds scale-up for coating TRISO nuclear fuel particles using Radioactive Particle Tracking (RPT)’, *Experimental Thermal and Fluid Science*, 80, pp. 90–104.
- Gamliel, D.P., Du, S., Bollas, G.M. and Valla, J.A. (2015) ‘Catalytic pyrolysis of miscanthus × giganteus in a spouted bed reactor’, *Bioresource Technology*, 191, pp. 187–196.
- Antunes, G.G.B., Bück, A., Mariano, F.P., Girardi, A.G. and Dos Santos, D.A. (2024) ‘Particle dynamics in a pseudo-2D spouted bed: Experiments and Euler–Lagrange simulations’, *Chemical Engineering Journal*, 491, 152007.
- Araújo dos Santos, D., Baluni, S. and Bück, A. (2020) ‘Eulerian Multiphase Simulation of the Particle Dynamics in a Fluidized Bed Opposed Gas Jet Mill’, *Processes*, 8(12), p. 1621.
- Boujjat, H., Rodat, S., Chuayboon, S. and Abanades, S. (2020) ‘Experimental and CFD investigation of inert bed materials effects in a high-temperature conical cavity-type reactor for continuous solar-driven steam gasification of biomass’, *Chemical Engineering Science*, 228, 115970.
- Foong, S.K., Lim, C.J. and Watkinson, A.P. (1980) ‘Coal gasification in a spouted bed’, *The Canadian Journal of Chemical Engineering*, 58, pp. 84–91.
- Wu, F., Yue, K., Gao, W., Gong, M., Ma, X. and Zhou, W. (2020) ‘Numerical simulation of semi-dry flue gas desulfurization process in the powder-particle spouted bed’, *Advanced Powder Technology*, 31(1), pp. 323–331.

Du, J., Wu, F. and Ma, X. (2023) 'Progress in research of process intensification of spouted beds: A comprehensive review', *Chinese Journal of Chemical Engineering*, 62, pp. 238–260.

Hooshdaran, B., Hosseini, S.H., Haghshenasfard, M., Nasr Esfahany, M. and Olazar, M. (2017) 'CFD modeling of heat transfer and hydrodynamics in a draft tube conical spouted bed reactor under pyrolysis conditions: Impact of wall boundary condition', *Applied Thermal Engineering*, 127(1), pp. 224–232.

Orozco, S., Alvarez, J., Lopez, G., Artetxe, M., Bilbao, J. and Olazar, M. (2021) 'Pyrolysis of plastic wastes in a fountain confined conical spouted bed reactor: Determination of stable operating conditions', *Energy Conversion and Management*, 229, 113768.

Martins, G.Z., Souza, C.R.F., Tumuluru, J.S. and Oliveira, W.P. (2007) 'Effect of process variables on fluid dynamics and adhesion efficiency during spouted bed coating of hard gelatine capsules', *Chemical Engineering and Processing: Process Intensification*, 46, pp. 313–321.

Sutkar, V.S., Hunsel, T.J.K.V., Deen, N.G. and Kuipers, J.A.M. (2015) 'Experimental and numerical investigations of a pseudo-2D spout fluidized bed with draft plates', *Powder Technology*, 270, pp. 537–547.

Mathur, K.B. and Gisher, P.E. (1955) 'A technique for contacting gases with coarse solid particles', *AIChE Journal*, 1(2), pp. 157-164.

San José, M.J., Alvarez, S., Morales, A., Olazar, M. and Bilbao, J. (2006) 'Solid cross-flow into the spout and particle trajectories in conical spouted beds consisting of solids of different density and shape', *Chemical Engineering Research and Design*, 84(6), pp. 487-494.

Yue, Y., Shen, Y., et al. (2021) 'CFD-DEM study of mitigation of alternating spout deflection in a spout fluidized bed', *Powder Technology*, 394, pp. 278-289.

Mathur, K.B. and Epstein, N. (1974) *Spouted Beds*. New York: Academic Press.

Sutkar, V.S., Deen, N.G. and Kuipers, J.A.M. (2013) 'Spout fluidized beds: Recent advances in experimental and numerical studies', *Chemical Engineering Science*, 86, pp. 124-136.

Zhong, W., Zhang, Y. and Jin, B. (2016) 'Particle circulation behavior in spouted beds with different geometries', *Powder Technology*, 301, pp. 1265-1274.

San José, M.J., Alvarez, S., Morales, A., Olazar, M. and Bilbao, J. (2006) 'Solid cross-flow into the spout and particle trajectories in conical spouted beds', *Chemical Engineering Research and Design*, 84(6), pp. 487-494.

- Hosseini, S.H., Zivdar, M. and Rahimi, R. (2009) 'CFD simulation of gas-solid flow in a spouted bed with a non-porous draft tube', *Chemical Engineering and Processing: Process Intensification*, 48(11), pp. 1539-1548.
- Olazar, M., San José, M.J., Aguayo, A.T., Arandes, J.M. and Bilbao, J. (1993) 'Stable operation conditions for gas-solid contact regimes in conical spouted beds', *Industrial & Engineering Chemistry Research*, 32(11), pp. 2826-2834.
- Sutkar, V.S., Deen, N.G. and Kuipers, J.A.M. (2013) 'Spout fluidized beds: Recent advances in experimental and numerical studies', *Chemical Engineering Science*, 86, pp. 124-136.
- Jittanit, W., Szrednicki, G. and Driscoll, R. (2010) 'Seed drying in fluidized and spouted bed dryers', *Drying Technology*, 28(10), pp. 1213–1219.
- Ostrovskij, N. (2014) 'Drying of polymer powder in fluidized bed: Modeling of multizone dryer', *Hemjska Industrija*, 68(6), pp. 651–671.
- Kunii, D. and Levenspiel, O. (1991) *Fluidization Engineering*. 2nd edn. Boston: Butterworth-Heinemann.
- Sutkar, V.S. et al. (2013) 'Experimental and computational study of gas–solid fluidization and spouting', *Powder Technology*, 246, pp. 656–663.
- Zhou, L., Zhang, L., Bai, L., Shi, W., Li, W., Wang, C. and Agarwal, R. (2017) 'Experimental study and transient CFD/DEM simulation in a fluidized bed based on different drag models', *RSC Advances*, 7(21), pp. 12764–12774.

## Appendix

### Appendix 1. Granular injection file

```
clc; clear;
```

```
%% Geometry domain extent
```

```
x_min = -0.15; x_max = 0.15;
```

```
y_min = 0.0; y_max = 1.7;
```

```
z_min = -0.1; z_max = 0.1;
```

```
num_particles = 36000; % Total number of particles
```

```
particle_diameter = 2e-3; % Particle diameter (2 mm)
```

```
particle_density = 1550; % Particle density (kg/m3)
```

```
particle_temperature = 25 + 273.15; % Initial temperature (K)
```

```
volume_single = (4/3)*pi*(particle_diameter/2)^3;
```

```
mass_single = particle_density * volume_single;
```

```
total_mass = mass_single * num_particles;
```

```
stop_time = 50; % Stop injection time (seconds)
```

```
mass_flow_total = total_mass / stop_time; % Total mass flow rate (kg/s)
```

```

mass_flow_per_particle = mass_flow_total / num_particles; % Single particle mass flow
rate

%% Set injection height (bottom 2 ~ 8 cm)

y_start = y_min + 0.02;

y_end = y_min + 0.08;

%% Randomly generate particle positions

x_pos = (x_max - x_min) * rand(num_particles,1) + x_min;

y_pos = (y_end - y_start) * rand(num_particles,1) + y_start;

z_pos = (z_max - z_min) * rand(num_particles,1) + z_min;

%% Write the injection file (double brackets + injection:0 per line)

filename = 'particle_injection_100s.inj';

fileID = fopen(filename, 'w');

for i = 1:num_particles

    fprintf(fileID, '((%.6f %.6f %.6f %.2f %.2f %.2f %.6f %.3f %.6e) injection:0)\n', ...

        x_pos(i), y_pos(i), z_pos(i), ...

        0.0, 0.0, 0.0, ... % Speed is 0

        particle_diameter, ...

        particle_temperature, ...

        mass_flow_per_particle);

end

```

```
fclose(fileID);
```

```
fprintf('\n  Injection file generated: %s\n', filename);
```

```
fprintf(' Total mass = %.4f kg\n', total_mass);
```

```
fprintf(' Stop injection time = %.1f s, mass flow rate per particle = %.6e kg/s\n', stop_time,
mass_flow_per_particle);
```

Appendix 2 Calculate the pressure drop of case 1

mixture

Average of Facet Values

Absolute Pressure [Pa]

---

plane-0.1	101314.21
plane-0.2	101313.86
plane-0.3	101312.37
plane-0.4	101313.85
plane-0.5	101314.44
plane-0.6	101317.65
plane-0.7	101320.26
plane-0.8	101322.01
plane-0.9	101323.91
plane-1.0	101324.54
plane-1.1	101324.91

plane-1.2	101325.06
plane-1.3	101325.04
plane-1.4	101325.02
plane-1.5	101325.02
plane-1.6	101325.01
plane-1.7	101325

-----

Net            101321.75

### Appendix 3 Calculate the pressure drop of case 2

mixture

#### Average of Facet Values

Absolute Pressure            [Pa]

-----

plane-0.1	101316.42
plane-0.2	101315.68
plane-0.3	101314.88
plane-0.4	101315.39
plane-0.5	101316.4
plane-0.6	101319.66
plane-0.7	101322.62
plane-0.8	101324.01
plane-0.9	101324.65
plane-1.0	101324.86

plane-1.1	101324.97
plane-1.2	101325.04
plane-1.3	101325.04
plane-1.4	101325.03
plane-1.5	101325.02
plane-1.6	101325.01
plane-1.7	101325

-----

Net	101321.75
-----	-----------

Appendix 4 Calculate the pressure drop of case 3

mixture

Average of Facet Values

Absolute Pressure	[Pa]
-------------------	------

-----

plane-0.1	101324.1
plane-0.2	101322.5
plane-0.3	101322
plane-0.4	101322.2
plane-0.5	101322.5
plane-0.6	101323.1
plane-0.7	101323.6
plane-0.8	101324.1
plane-0.9	101324.6

plane-1.0	101324.7
plane-1.1	101324.8
plane-1.2	101324.9
plane-1.3	101325.04
plane-1.4	101325.03
plane-1.5	101325.02
plane-1.6	101325.01
plane-1.7	101325

-----

Net	101321.75
-----	-----------